Solar Energy 300 (2025) 113817

Contents lists available at ScienceDirect

Solar Energy

journal homepage: www.elsevier.com/locate/solener

Interface passivation of a hole transporting material in order to improve the efficiency of perovskite solar cells

Jędrzej Szmytkowski [a,*], Cheng-Gang Huang [b], Satish Bykkam [a], Damian Glowienka [a,*], Yulia Galagan [b,c,*]

[a] Faculty of Applied Physics and Mathematics, Gdańsk University of Technology, Narutowicza 11/12, 80-233 Gdańsk, Poland
[b] Department of Materials Science and Engineering, National Taiwan University, Taipei 10617, Taiwan
[c] TNO, Materials Solutions, High Tech Campus 25, Eindhoven 5656 AE, Netherlands

ARTICLE INFO

Keywords:
Perovskites
Energy efficiency
Solar cells
Photovoltaics

ABSTRACT

In this study, we evaluate three distinct materials (PTAA, P3HT and P3HT-COOH) applied as passivation layers in combination with Cu:NiO_x, which serves as a hole transporting layer (HTL) in organic–inorganic perovskite solar cells (PSCs). The investigation revealed that the solvent used for a perovskite precursor (DMF:DMSO) exhibited the lowest contact angle on the P3HT-COOH. It leads to a smoother perovskite surface prepared on this passivation layer in a comparison to samples with PTAA and P3HT. Photoluminescence spectra analysis indicated a superior quenching efficiency in the HTL/perovskite configurations employing P3HT-COOH, slightly outperforming those with PTAA. This suggests an enhanced hole transfer from the perovskite to the HTL. PSCs constructed with a dual-cation perovskite $Cs_{0.15}FA_{0.85}Pb(I_{0.95}Br_{0.05})_3$ and various passivation layers were also fabricated. The results showed that devices with the P3HT-COOH exhibited the lowest hysteresis index and achieved the highest power conversion efficiency, underscoring the potential of P3HT-COOH as an effective passivation layer for PSCs.

1. Introduction

Currently, we observe intensive efforts directed toward the improving of an efficiency and a stability of perovskite solar cells (PSCs) [1]. A typical structure of the PSC includes a hole transporting layer (HTL) and an electron transporting layer (ETL) located at both sides of a perovskite material. It seems that the usage of an interface passivation layer between the perovskite and the HTL (or ETL) should help to achieve a better efficiency and stability [2]. The reason is that a passivation material can limit the possible degradation reaction mechanism. Additionally, it acts as a surface modifier to provide a better surface property for the coating process of a perovskite during the device preparation.

One of the materials employed as the HTL in PSCs is Cu:NiO_x, where the nickel oxide (NiO_x) is doped with a copper to improve a conductivity. Recently, it has been demonstrated that the poly[bis(4-phenyl)(2,4,6-trimethylphenyl)amine (PTAA) serves as a good intermediary layer between Cu:NiO_x and the $MAPbI_3$ perovskite [3]. However, the high cost and substantial hydrophobicity of PTAA, which lead to coverage challenges in the inverted architecture, have prompted researchers to explore more affordable passivation materials [4].

Here, two other polymer materials have been selected to be coated on Cu:NiO_x as a passivation layer. One of them is poly(3-hexylthiophene-2,5-diyl) (P3HT), which is commonly used as a donor in organic photovoltaics. The latter is poly[3-(6-carboxyhexyl)thiophene-2,5-diyl] (P3HT-COOH) [5,6], which structure is based on P3HT but it has an extra carboxylic groups at the end of the side chains [7]. In this work, we have decided to compare all the above mentioned passivation materials (PTAA, P3HT and P3HT-COOH) in order to find the most effective passivation layer for PSC's. The molecular structures of these polymers are shown in Fig. 1.

It should be mentioned that perovskite solar cells with self-assembled molecules were recently investigated [8,9]. A role of self-organized molecules in PSCs is to use them as selective contacts, where an achievement of desirable energy levels and dipoles at interfaces allows to obtain a better charge transfer. Thus, this effect plays a different role than in dye-sensitized solar cells [10–16], where the self-assembled materials increase a photon capture cross section and lead to a better harvesting of light. We should note that the self-organization of molecules has been recently observed in P3HT-COOH [17,18]. Therefore, this compound became much more attractive to use it in PSCs.

* Corresponding authors.
E-mail addresses: jedszmyt@pg.edu.pl (J. Szmytkowski), damian.glowienka@pg.edu.pl (D. Glowienka), yulia.galagan@tno.nl (Y. Galagan).

https://doi.org/10.1016/j.solener.2025.113817
Received 3 April 2025; Received in revised form 16 July 2025; Accepted 21 July 2025
Available online 6 August 2025

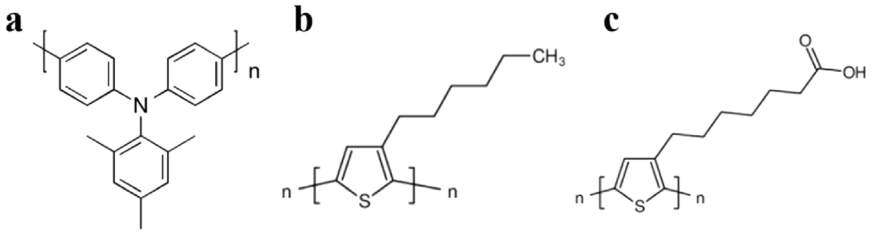

Fig. 1. Molecular structures of passivation materials: (a) PTAA, (b) P3HT and (c) P3HT-COOH.

In this work, the dual cation (2C) perovskite $Cs_{0.15}FA_{0.85}Pb(I_{0.95}Br_{0.05})_3$ was applied to fabricate solar cells. Such a type of 2C perovskite has been recently studied in our recent works [19–21].

2. Experimental section

2.1. Cleaning of substrates

Tin doped indium oxide (ITO) (7 Ohm/sq, Ruilong) substrates were cleaned with a soap water solution and placed for 10 min under sonication. Then, the solution has been changed to the mixture by blending 10 mL of ammonia (35%, Fisher) and 10 mL hydrogen peroxide (35%, Acros) solutions in 40 mL of deionized water. The obtained mixture solution was sonicated for 30 min. The next step was to sonicate the substrates in methanol (99.99%, Burdick & Jackson) and later in isopropanol (IPA) (99.99%, Burdick & Jackson), both for 30 min. Subsequently, the substrates were dried with N_2 gas spray and cleaned for 15 min in plasma oven on a high power.

2.2. Solution preparation

0.1 M Cu:NiO_x (5% Cu) was prepared by dissolving $Ni(NO_3)_2{\cdot}6H_2O$ (98%, Alfa Aesar) and $Cu(NO_3)_2{\cdot}3H_2O$ (99%, Sigma Aldrich) in 2-methoxylethanol:acelyacetone solution with the ratio 9:1 by volume and was sonicated to make sure it was completely dissolved. Here, we used solvents: 2-methoxyethanol (99%, Alfa Aesar) and acelyacetone (99%, Kanto Chemicals). Regioregular P3HT (M_w = 50-70 k, Rieke Metal) solution was prepared by dissolving 1 mg of P3HT directly in 1 mL of chlorobenzene (CB) (>99%, Acros) and diluted to a certain concentration before coating. PTAA (M_w = 5-20 k, Solaris Chem) solution was obtained with toluene (>99.8%, Acros) with a concentration 8 mg/mL and later diluted to 2 mg/mL before use. P3HT-COOH (M_w = 50-60 k, Rieke Metal) was dissolved in N,N-dimethylformamide (DMF) (99.8%, Acros) with a concentration of 1.5 mg/mL, stirred over a week and sonicated several times to make sure that the P3HT-COOH was completely dissolved. After that it was diluted to a certain concentration before coating.

In order to prepare the perovskite with the formula $Cs_{0.15}FA_{0.85}Pb(I_{0.95}Br_{0.05})_3$, the following procedure was applied. Cesium bromide (CsBr) (99.999%, TCI), formamidinium iodide (FAI) (>99.99%, GreatCell Solar) and lead iodide (PbI_2) (99.999%, TCI) were dissolved in DMF:DMSO solution with the ratio 4:1 by volume, where DMSO is an abbreviation of dimethyl sulfoxide (99.7%, Acros). [6,6]-phenyl C_{61} butyric acid methyl ester (PCBM) (>99%, Solenne) was prepared by dissolving the powder in CB with a concentration of 20 mg/mL. Both these solutions were later stirred overnight at room temperature in the glovebox. The stock solution of polyethylenimine (PEI) (99.9%, Alfa Aesar) was obtained by dissolving PEI in IPA with a concentration of 8 wt% and after that it was diluted to 0.1 wt% and stirred overnight before use.

2.3. Device fabrication

The HTL layer (Cu:NiO_x) was deposited by a static spin-coating (1500 rpm, 1500 rpm/s, 60 s) and annealed using a two-step method: first at 150° C for 5 min in the glovebox and later at 300° C for 15 min in ambient air to achieve a complex phase transformation. P3HT was spin-coated with a 4000 rpm speed for 30 s and 4000 rpm/s acceleration, then annealed at 100° C for 10 min. PTAA was deposited with a 5000 rpm for 30 s with 5000 rpm/s and subsequently annealed at 100° C for 10 min. P3HT-COOH was spin-coated (4000 rpm, 4000 rpm/s, 35 s) and annealed at 150° C for 20 min to fully remove the solvent. All these passivation layers were prepared in the glovebox.

For the fabrication of a perovskite layer, the spin-coating combined with an anti-solvent method was used. The process started with a 1000 rpm rotational speed for 5 s with an acceleration 200 rpm/s and later with a 5000 rpm for 30 s with 5000 rpm/s acceleration. At the 15th second of the second step, CB was dropped onto the sample to facilitate the formation of an intermediate phase of the perovskite. After the spin-coating of the perovskite layer at 110° C, annealing process was used for 20 min to form the perovskite crystal.

Here, due to the hydrophobic properties of PTAA and P3HT layers, the dynamic spin-coating method was applied for these samples. It means that during preparation of the perovskite layer, a high amount of the perovskite solution was dropped onto a sample after 3 s from starting the spin-coating process. The regular static spin-coating technique was used for a sample with P3HT-COOH. The ETL material (PCBM) was deposited (1000 rpm, 1000 rpm/s, 30 s) without annealing. After that, PEI (a work function modifier) was spin-coated with a 3000 rpm speed for 30 s with an acceleration 3000 rpm/s. Lastly, 100 nm of a silver slug (99.99%, Gredmann) was thermal evaporated on the top of samples under a pressure lower than 5×10^{-6} Torr to create the electrode with an active area of 0.09 cm^2. Architecture of a complete PCS is shown in Fig. 2.

2.4. Characterization

The morphology of surfaces was investigated using the scanning electron microscope (SEM) (JEOL, JSM-7800F) and the atomic force microscope (AFM) (Bruker, OMV-NTSC). Photoluminescence (PL) spectra were recorded with a system created by CL-technology (model Uninanotech). The ultraviolet photoelectron spectroscopy (UPS) measurements were performed using the PHI 5000 VersaProbe III system (ULVAC-PHI Inc.) equipped with a He I ultraviolet source (21.2 eV). The goniometer (Sindatek, model 100SB) has been used to determine the contact angles. The external quantum efficiency (EQE) spectra were measured with the IPCE instrument (LiveStrong, model LSQE-R). The solar simulator (Yamashita Denso, model YSS-50A-400A) has been applied to illuminate samples. In order to record the J-V characteristics, a source measure unit (Keithley 2400) has been used. These measurements were done in N_2 environment.

The J-V characteristics have been obtained for two applied voltage directions. The first scan was recorded in the reverse direction (from 1.2 V to −0.2 V) and the second scan in the forward one (from −0.2 V

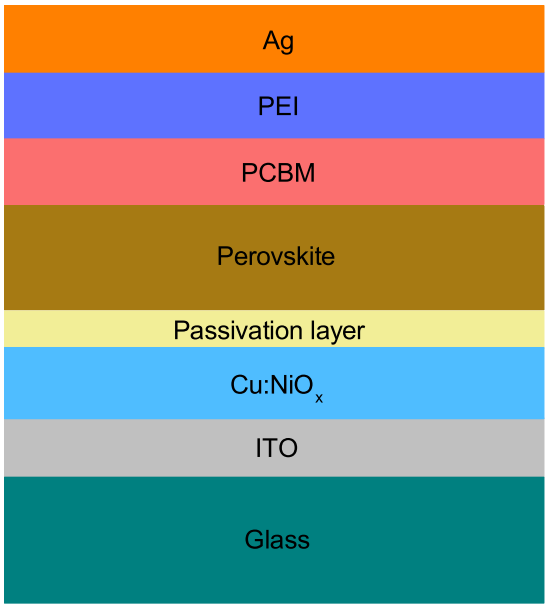

Fig. 2. The architecture of solar cells studied in this work.

to 1.2 V). Therefore, the hysteresis effect could be determined. Both scans were measured with a scanning rate equal to 0.165 V s^{-1} with 20 mV step and with 2 min of light soaking preconditioning.

The representative solar cells were selected to find the maximum power point tracking (MPPT). Here, we continuously illuminated these samples for 120 s with the control of current and voltage.

2.5. Simulation model

To simulate photoelectrical properties of PSCs, the drift–diffusion model with the Shockley–Read–Hall, the Auger and the modified Langevin recombination mechanisms has been used. The mathematical description of the model and applied numerical methods were presented in details in our previous papers [19,21,22]. We should mention that the dynamical effects of ions were not taken into account in these simulations. The reason is that only steady-state conditions have been considered here and, for such a case, ions influence the PSCs negligibly [22].

For the hole transporting layer (Cu:NiO_x) [23–25], the electron transporting layer (PCBM) [26–30] and an active layer (a perovskite material) [19,31], the electrical parameters were adopted from the literature. To determine the generation profile of samples, the optical transfer-matrix model [32–34] has been used. Such a generation profile was calculated with values of real and imaginary refractive indices drawn versus wavelengths for Cu:NiO_x, perovskite and PCBM [3].

3. Results and discussion

3.1. Hydrophobicity of passivation layers

In order to determine the surface hydrophobicity, the contact angle of a pure DMF:DMSO (1:4 volume ratio) on the top of passivation materials was measured. It should be reminded that DMF:DMSO serves as a solvent for a perovskite precursor. Here, the investigated samples had a structure: passivation layer/Cu:NiO_x/glass. Fig. 3 shows results obtained for samples with investigated compounds (PTAA, P3HT and P3HT-COOH) and for a sample without a passivation layer. For the latter, the contact angle was measured directly on the Cu:NiO_x surface. In the following, we will use the notation 'None' for all types of samples (including solar cells) without a passivation material.

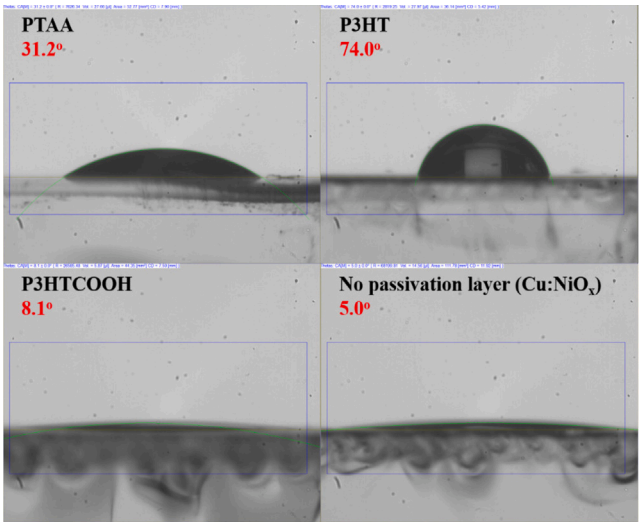

Fig. 3. The contact angles of DMF:DMSO dropped on PTAA, P3HT, P3HT-COOH and Cu:NiO_x materials.

In Fig. 3, we can see that contact angles of DMF:DMSO on the PTAA and P3HT films have values 31.2° and 74.0°, respectively. The first thing immediately affected by a contact angle is the quality of the subsequent coating, leading to difficulty in obtaining a good film on the surface with a low contact angle. If we use a regular static spin-coating method for the perovskite layer deposited on the top of films characterized by the highest contact angles (PTAA and P3HT), then we observe a coverage problem, as demonstrated in Figure S1. It induces formation of numerous pinholes with a direct impact on the shunt resistance, leading to an inefficient and worrisome fabrication process. Therefore, a dynamic coating method was used for this kind of samples by dropping the perovskite precursor solution, when the spin process already started. Thus, the centrifugal force and the pressure caused by the dropping solution assist the solution to be deposited on substrates with a better coverage. However, it should be noted that this method is not as stable as a regular static spin-coating. The reason is that the timing of a dropping solution is hard to control. Also, the dropping pressure can be treated as an another unstable factor during the dynamic spin-coating.

The contact angles for the 'None' and P3HT-COOH samples are 5.0° and 8.1°, respectively. Thus, we can see a huge difference between samples with P3HT and P3HT-COOH, meaning that carboxylic groups on the end of a side chains can largely change the wetting property of a thin film. Also, P3HT-COOH has a surface energy that is closer to Cu:NiO_x. It causes a full coverage of a perovskite layer and gives a better reproductivity from batch to batch.

3.2. Surface morphology studies

The SEM and AFM images of perovskite surfaces fabricated on different passivation layers are presented in Figs. 4 and 5, respectively. Here, the investigated samples had a structure: perovskite/passivation layer/Cu:NiO_x/glass. We found a correlation between the root mean square roughness (Rq) of perovskite surfaces and the contact angle described in the previous paragraph.

The P3HT layer characterized by the highest contact angle (74.0°) causes a high roughness (Rq = 18.1 nm) of a perovskite layer deposited on the top of P3HT surface. Therefore, the insufficient contact between the perovskite and the HTL can occur in such a sample. In the solar cells, it might even lead to shunted effects consequently lowering the device performance. Comparing with other samples, the relative smaller grain size of a perovskite observed for the P3HT sample means

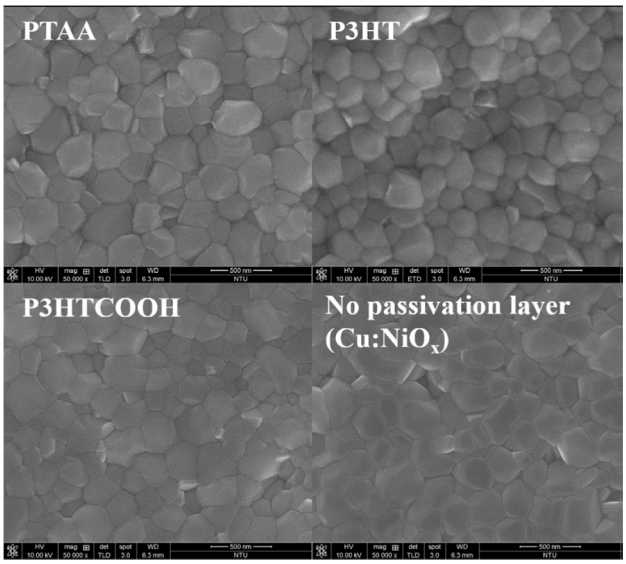

Fig. 4. SEM images of perovskite films coated on the top of PTAA, P3HT, P3HT-COOH and Cu:NiO_x materials.

that more grain boundaries were formed in the bulk. These boundaries can act as recombination centers for electrons and holes, decreasing the diffusion length of charge carriers. As a consequence, they limit the number of carriers that are generated by the perovskite layer.

Furthermore, the PTAA layer (with a high value of contact angle of 31.2°) also causes a rough surface of a perovskite prepared on the PTAA (Rq = 18.1 nm). Consistently, in a comparison to the samples with P3HT and PTAA, the much smoother perovskite surfaces were obtained for the P3HT-COOH (Rq = 17.4 nm) and 'None' (Rq = 17.3 nm) samples. For both materials (P3HT-COOH and not passivated Cu:NiO_x), we obtained the lowest values of contact angles. It confirms a correlation between the contact angle of DMF:DMSO solvent on the passivation layer and the roughness of a perovskite surface deposited on the top of this passivation material.

3.3. Photoluminescence studies

The PL measurements have been conducted in perovskite/passivation layer/Cu:NiO_x/glass structures, where the perovskite layer absorbs photons. In such a system, generated holes are immediately extracted through Cu:NiO_x (which serves as a HTL in PSCs) and suppress the emission of luminescence from the sample.

Fig. 6 presents the PL results obtained for samples with different passivation layers. We can see that all peaks are located at the same wavelength. It clearly shows that there are no band-gap shifts for the perovskite in investigated samples. The intensity of PL can indicate the extraction capability of HTL in such systems. The highest peak is observed for the sample with P3HT. It means that the worst hole extraction occurs for this sample, which has even worse properties than a not passivated Cu:NiO_x material. Low PL intensities observed for the P3HT-COOH (the lowest) and PTAA samples are a consequence of a good quenching efficiency, suggesting that a faster hole transfer may occur at the HTL/perovskite interface, when these materials are incorporated.

3.4. Optimization of passivation layers

In this work, photovoltaic devices with the architecture of ITO/Cu:NiO_x/passivation layer/ $Cs_{0.15}FA_{0.85}Pb(I_{0.95}Br_{0.05})_3$/PCBM/PEI/Ag were studied. However, to obtain a better comparison between the passivation layers, the concentrations of solutions with passivation materials should be optimized.

The solar cells performance with the P3HT layer is shown in Figure S2. Here, four photovoltaic parameters (a power conversion efficiency (PCE), a short-circuit current (J_{sc}), an open-circuit voltage (V_{oc}) and a fill factor (FF)) are illustrated for three concentrations of P3HT (0.25 mg/mL, 0.125 mg/mL and 0.05 mg/mL). We can see a clear trend that PCE decreases with the decreasing of a P3HT concentration. The worse performances for lower concentrations were largely stemmed from the high current loss. It can be explained that, when the P3HT layer becomes thinner or it even cannot fully cover the substrate, the possibility of a direct contact between Cu:NiO_x and the perovskite increases. Then, the degradation reaction can occur at the interface which, consequently, lowers both the current and the FF of devices. It should be mentioned that, if the concentration of P3HT was higher than 0.25 mg/mL, then it was almost impossible to cover the top of a sample due to a high contact angle of the perovskite precursor solution on the top of P3HT film (even when the dynamic coating method was used). This is a reason why we decided to investigate solar cells with maximum 0.25 mg/mL concentration of P3HT.

Figure S3 shows the results for PCE, J_{sc}, V_{oc} and FF obtained for three concentrations of P3HT-COOH (0.25 mg/mL, 0.5 mg/mL and 1 mg/mL). The device performance for 0.25 mg/mL and 0.5 mg/mL are almost the same, having the average PCE of (16.56 ± 0.52) % and (16.69 ± 0.61) %, respectively. The observed a small difference might be due to the discrepancy from batch to batch. The PCE starts to decrease, when the concentration increases up to 1 mg/mL. It shows around 1% lower value in a comparison to the average PCEs for 0.25 mg/mL and 0.5 mg/mL samples. This effect originates from a little bit lower J_{sc} and FF. We decided to choose 0.5 mg/mL concentration of P3HT-COOH to compare solar cells with different passivation layers.

The concentration for the device with PTAA was optimized in our previous work [3], where the best performance of PSCs was obtained for the PTAA concentration equal to 2 mg/mL.

3.5. UPS studies

Figure S4 presents the UPS results for the secondary electron cutoff region (left) and the valence band region (right) obtained for the following configurations: Cu:NiO_x, Cu:NiO_x/PTAA (denoted here as PTAA), Cu:NiO_x/P3HT (denoted as P3HT) and Cu:NiO_x/P3HT-COOH (denoted as P3HT-COOH). In all samples, the Cu:NiO_x layer was used as the base, ensuring consistent device architecture throughout the study. The ionization energies were calculated as: (−4.644 ± 0.302) eV for Cu:NiO_x, (−4.938 ± 0.168) eV for PTAA, (−4.554 ± 0.078) eV for P3HT and (−5.147 ± 0.159) eV for P3HT-COOH. Similarly, the corresponding Fermi level positions (with respect to vacuum) were (−4.146 ± 0.204) eV for Cu:NiO_x, (−4.168 ± 0.199) eV for PTAA, (−3.938 ± 0.069) eV for P3HT and (−3.885 ± 0.134) eV for P3HT-COOH.

3.6. Comparison of devices

Fig. 7 presents the comparison of four photovoltaic parameters obtained for solar cells fabricated with different passivation layers. The samples with P3HT-COOH show a highest average PCE (16.69 ± 0.61) % than devices with PTAA (16.26 ± 0.42) %, P3HT (12.24 ± 0.52) % and without a passivation layer (13.56 ± 0.57) %. It looks that the best PCE obtained for the P3HT-COOH samples originates from the largely improved J_{sc} and FF compared to the P3HT and 'None' samples, which can come from a good perovskite crystallinity and a better hole extraction capability through HTL. Although the P3HT-COOH and PTAA devices have similar average PCEs, there is a visible difference in FF and V_{oc}. We can see that the P3HT-COOH samples have a higher average FF (77.96 ± 1.71) %, whereas the PTAA samples are characterized by a lower FF (73.49 ± 2.54) %. For the case of an open-circuit voltage, the PTAA devices have a higher average V_{oc} (1.00 V) than the P3HT-COOH cells (0.96 V).

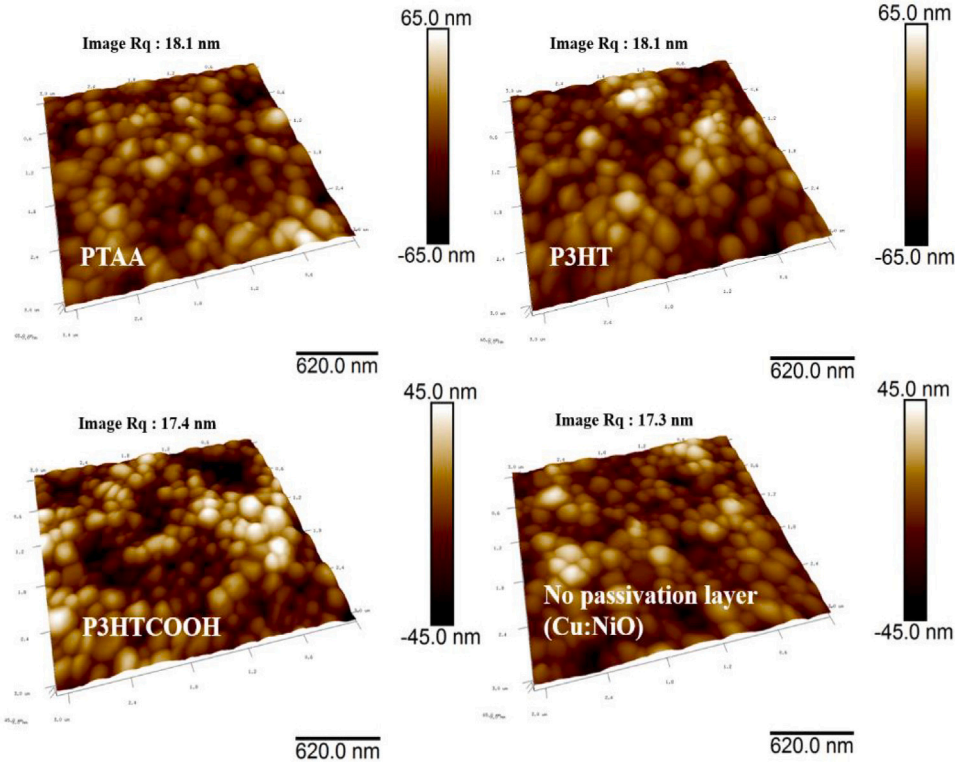

Fig. 5. AFM height images with the root mean square roughness (Rq) of perovskite films coated on the top of PTAA, P3HT, P3HT-COOH and Cu:NiO_x materials.

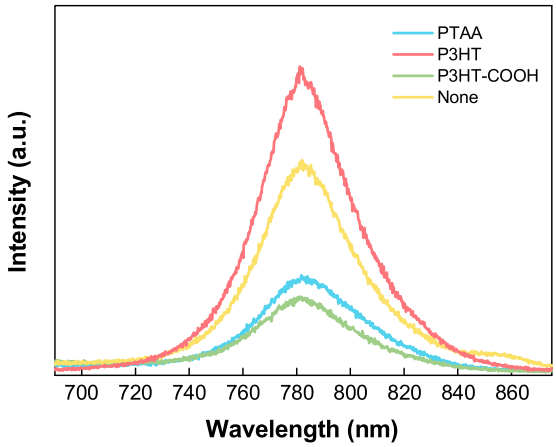

Fig. 6. The steady-state photoluminescence spectra of perovskite films coated on different passivation materials.

It is seen that the 'None' samples indicate a better performance comparing to the P3HT devices. The reason is that the solvent (CB) used for P3HT plays a role of an anti-solvent for the perovskite. Therefore, even after the annealing process, it still could worsen the interface and leads to a worse perovskite crystallinity.

The current–voltage curves for representative photocells are shown in Fig. 8. The corresponding performance parameters are summarized in Table 1 including the hysteresis index (HI), which is defined as

$$HI = \frac{(PCE_{Reverse} - PCE_{Forward})}{PCE_{Reverse}}, \quad (1)$$

where $PCE_{Reverse}$ and $PCE_{Forward}$ are PCEs measured for the reverse and the forward directions, respectively. We can see that the P3HT-COOH sample has the lowest hysteresis index (1.1%) indicating its smoother transport properties. The HI is higher for other samples but the obtained values (2.4–3.5%) are still in a very low level.

Table 1
Performance parameters for PSCs with different passivation layers.

Sample	Hysteresis index (%)	Scan direction	V_{oc} (V)	J_{sc} (mA cm^{-2})	FF (%)	PCE (%)
PTAA	3.0	Reverse	1.00	22.17	73.49	16.26
		Forward	0.99	22.05	72.02	15.77
P3HT	3.5	Reverse	0.92	18.03	73.79	12.24
		Forward	0.93	17.81	71.55	11.80
P3HT-COOH	1.1	Reverse	0.96	22.24	77.96	16.69
		Forward	0.96	22.15	77.60	16.51
'None'	2.4	Reverse	0.99	19.05	72.23	13.56
		Forward	0.98	18.90	71.25	13.23

Meanwhile, the reliability of the solar cells performance is further confirmed by MPPT presented in Fig. 9. We can see that the PTAA and P3HT-COOH samples show a good stability of PCE through the 120 s measurement. The P3HT and 'None' devices have a slightly gradually increased PCE during this whole period.

The EQE spectra for all solar cells are presented in Fig. 10. We can see that the P3HT-COOH sample shows an enhanced light response compared to the others. As a result, the P3HT-COOH device has a higher integrated current density of 21.86 mA/cm^2 compared to 21.51 mA/cm^2, 18.57 mA/cm^2 and 21.12 mA/cm^2 for the PTAA, P3HT and 'None' samples, respectively. This trend is consistent with the PL results, showing that the difference is largely due to the HTL/perovskite interface and the perovskite crystallinity. The patterns of obtained EQE curves are similar for the P3HT, P3HT-COOH and 'None' samples in a wavelength range from 300 to 650 nm. Only a down shift of the EQE to lower values observed for the P3HT and 'None' samples indicates that the current differences might be highly related to the perovskite bulk recombination. The curve for the PTAA sample is slightly different than for other devices. It looks that the EQE peaks for this device are slightly shifted towards the longer wavelengths. We also observe

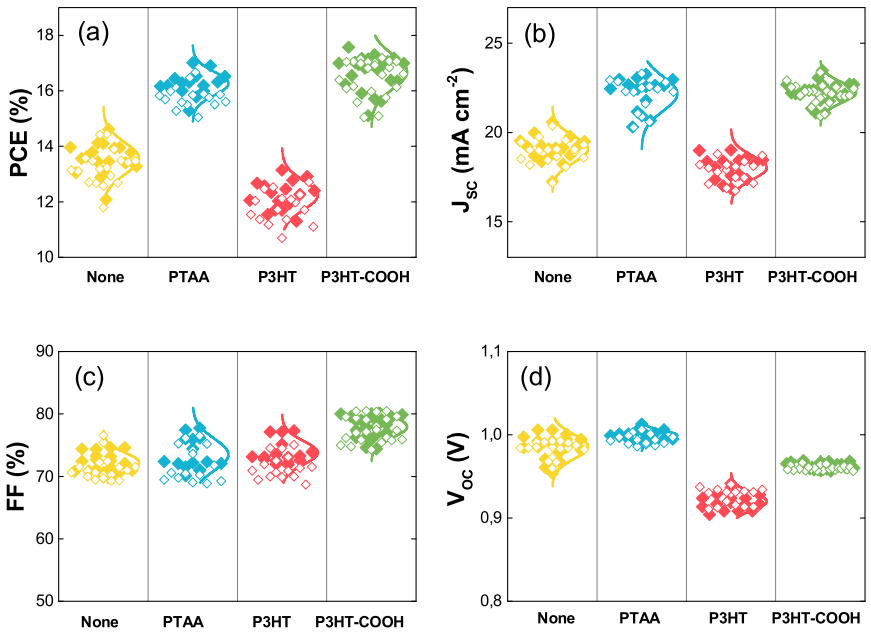

Fig. 7. Performance of solar cells with different passivation layers. Closed and open symbols show the reverse and the forward directions, respectively.

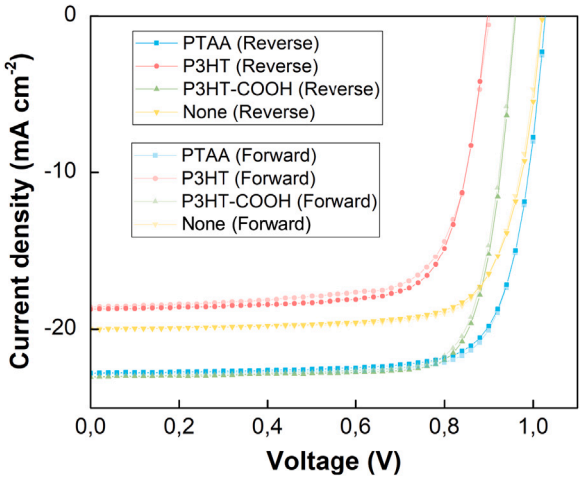

Fig. 8. Current–voltage curves for solar cells with different passivation layers.

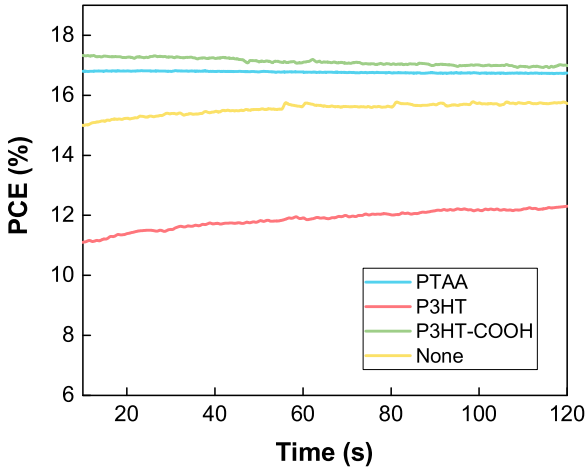

Fig. 9. The maximum power point tracking for solar cells with different passivation layers.

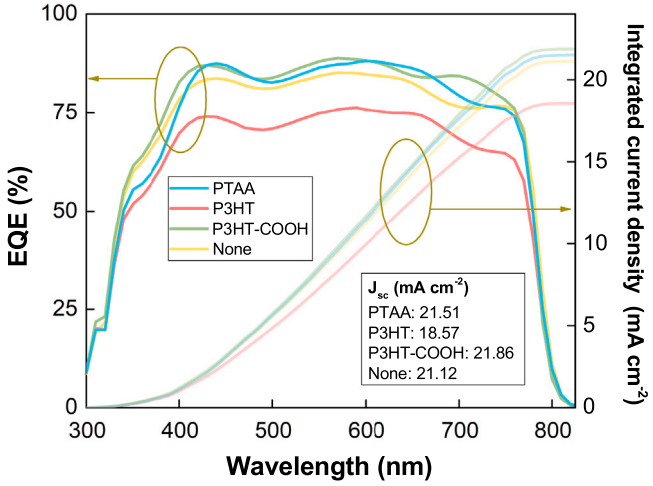

Fig. 10. The EQE spectra and the integrated current densities for solar cells with different passivation layers. An inset shows values of J_{sc} for these devices.

a significant loss of the EQE values at short (350–410 nm) and long (690–780 nm) wavelengths. This discrepancy might be related to the interface properties.

3.7. Light intensity analysis

In the following, we will focus on the light intensity analysis of the devices with different passivation layers. It should be noted that, recently, a detailed and stepwise guidance for such an analysis has been provided [35]. In this work, the light intensity characteristics were obtained by measuring the current–voltage curves under different illuminations (1, 0.1, 0.01 and 0.001 suns), which were controlled by neutral density (ND) filters.

The experimental results of J_{sc} versus a light intensity obtained for devices with different passivation layers are shown in Figure S5. We can see that J_{sc} is practically linear with the light intensity drawn in the log–log scale. This is a reason that we can present other photovoltaic parameters (V_{oc}, FF and PCE) as a function of J_{sc}, which can be treated

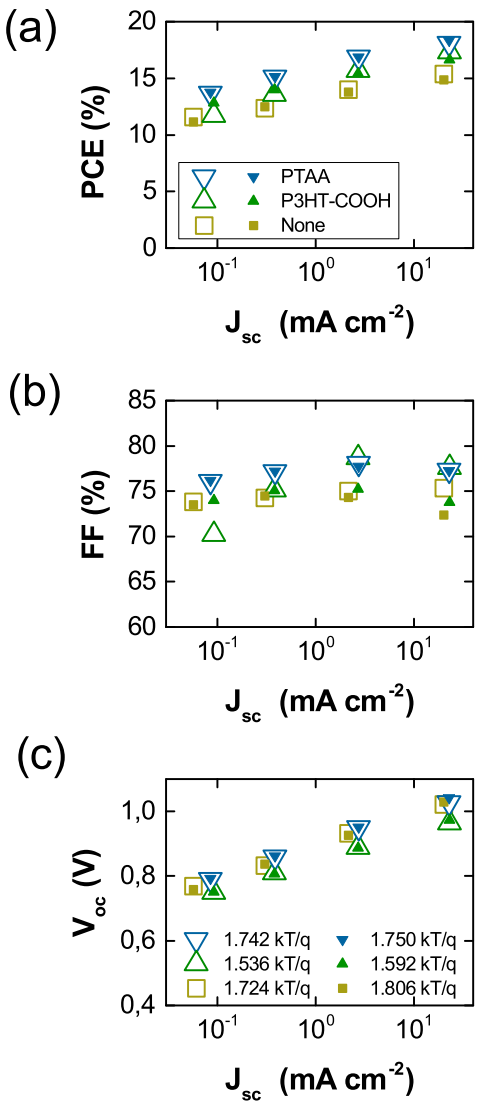

Fig. 11. The light intensity experimental (open symbols) and simulation (closed symbols) results drawn for solar cells with different passivation layers. The results are shown for PTAA (blue), P3HT-COOH (green) and 'None' (dark yellow) devices. (For interpretation of the references to colour in this figure legend, the reader is referred to the web version of this article.)

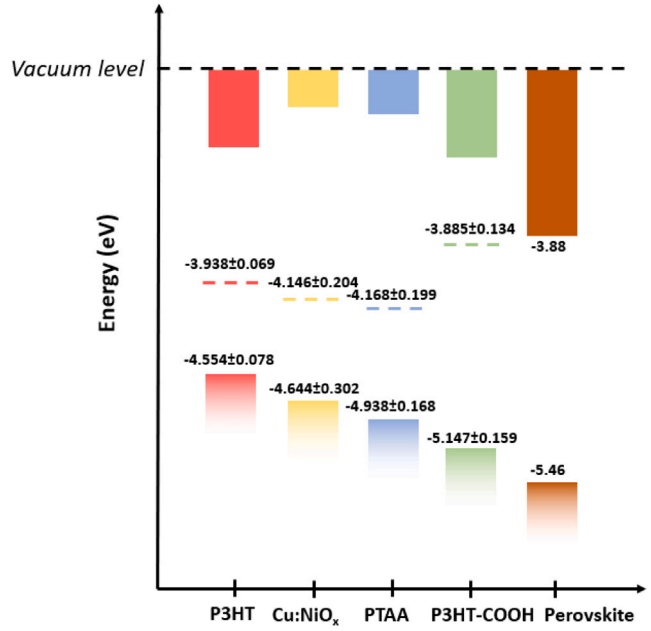

Fig. 12. Schematic energy level alignment between different HTLs and a perovskite material. The diagram is illustrative and not drawn to scale.

as an equivalent of the intensity of illumination. The obtained relations are presented in Fig. 11 for the PTAA, P3HT-COOH and 'None' devices. We decided to neglect such an analysis for the P3HT cell due to its weaker passivation properties in a comparison to other materials.

First, the FFs do not show a huge differences around 1 sun, meaning that there is no visible impact of series resistance for all samples. Also, it can be attributed to similar energy levels for all HTLs, which situation does not lead to any visible transport losses at the interface between HTL and a perovskite layer. The FFs of all devices show larger differences at lower light intensity, which can be more related to the bulk losses in the devices. It is clearly seen that the P3HT-COOH and PTAA samples indicate very similar values of FF in a high range of intensities. At a low light intensity, the P3HT-COOH sample has an observable drop by about 5%, if comparing to the PTAA sample. Such a behavior can be associated with a higher bulk recombination or the shunt resistance for the P3HT-COOH device in a comparison to the PTAA solar cell.

For the V_{oc} analysis, an ideality factor (n_{id}) has been calculated from the diode equation, which is related to a slope of V_{oc} versus J_{sc} presented in the semi-log scale. The obtained values of n_{id} (in kT/q units) are presented in Fig. 11c. The PTAA and 'None' samples have a high n_{id} with values close to 2 kT/q. It means that either interface losses should be lower or the bulk defects dominate in these devices. However, we would expect that Cu:NiO_x has a much higher interface recombination than the PTAA sample. For the P3HT-COOH sample, n_{id} value is around 1.5 kT/q and shows V_{oc} losses larger than 300 mV, if comparing to the Shockley–Queisser limit. Based on conclusions presented in the guideline [35], it could be explained that this sample suffers from a higher interface recombination.

In addition, Fig. 11 shows a comparison between experimental results and theoretical calculations based on the electrical drift–diffusion model. Tables 2 and 3 present physical parameters used in the modeling. The obtained goodness-of-fit was equal or higher than 98% for the PTAA, P3HT-COOH and 'None' devices. We can clearly see that the bulk defect concentration is the highest for the 'None' sample and decreases for solar cells with P3HT-COOH (slightly) and PTAA (strongly). In general, values above 10^{22} m^{-3} are considered as high bulk defect densities. Therefore, all samples suffer from relatively high bulk losses. However, the mobility of charge carriers in the bulk is very high and only the 'None' device has it lower than 18 cm^2 V^{-1} s^{-1}. Thus, a higher recombination rate or the transportation losses in the bulk are more visible for the 'None' PSCs.

The ETL and HTL interface trap densities are relatively small for the PTAA and 'None' samples. We have found much higher values of these densities for the P3HT-COOH device. For example, they are three orders of magnitude greater for the boundary between the ETL and the perovskite. It might lead to higher interface losses in this solar cell, especially observed at V_{oc}. The small shift of the energy levels appears for the 'None' sample. It can be attributed to a different position of the Cu:NiO_x valence band in a comparison to passivation layers.

3.8. Influence of the energy level alignment on photovoltaic properties

Fig. 12 shows an energy level alignment between different HTLs and a perovskite material. Here, diagrams for HTLs are presented with energy ionizations and Fermi levels found from the UPS measurements. The literature value of the valence band maximum for the perovskite

Table 2
Parameters used in simulation of the PSCs. Parameters for holes are written in brackets and for electrons without brackets.

Name	Unit	Cu:NiO_x (HTL)	2C perovskite	PCBM (ETL)
Thickness	nm	13	360	37.5
Permittivity		2.1	24.1	3.75
Mobility	$cm^2\ V^{-1}\ s^{-1}$	(0.01)	–	7.91×10^{-4}
Capture rate	$10^{-14}\ m^3\ s^{-1}$	–	1 (1)	–
Auger coefficient	$10^{-40}\ m^6\ s^{-1}$	–	1.55 (1.55)	–
Langevin prefactor		–	1.2×10^{-5}	–
Energy level	eV	–	−3.88 (−5.46)	−3.90
Doping concentration	m^{-3}	(1.20×10^{24})	0	0
Effective density of states	m^{-3}	2.5×10^{25}	1.2×10^{24}	2.5×10^{25}
Series resistance	$\Omega\ cm^2$		0.1	
Shunt resistance	$\Omega\ cm^2$		1.1×10^6	

Table 3
The fitted parameters obtained from the simulation of PSCs.

Name	Unit	PTAA	P3HT-COOH	'None'
Bulk trap density	$10^{22}\ m^{-3}$	2.91	4.79	4.92
2C perovskite mobility	$cm^2\ V^{-1}\ s^{-1}$	18.23	18.53	14.09
ETL interface trap density	$10^{14}\ m^{-2}$	1.8674	1433.6	1.2568
HTL interface trap density	$10^{14}\ m^{-2}$	7.512	183.99	64.909

is located around −5.46 eV [36]. We can see that the energy alignment between Cu:NiO_x, the organic HTL and the perovskite layer is most favorable for P3HT-COOH. In contrast, the largest hole extraction barrier exists in the Cu:NiO_x/P3HT/perovskite system, which correlates with the lowest J_{sc} values observed among all tested samples. On the other hand, the best energetic alignment has been achieved for the P3HT-COOH-based architecture, which corresponds to the highest J_{sc} values in our study. This performance trend strongly supports the interpretation that interfacial energy level alignment should be a key factor driving a charge extraction efficiency in these devices.

Interestingly, the Fermi level of P3HT-COOH (−3.885 ± 0.134) eV is very close to the reported conduction band minimum of the perovskite layer (around −3.88 eV [36]). This alignment may create an unintended electron extraction pathway from the perovskite to the HTL, increasing the likelihood of interfacial recombination. This interpretation is consistent with our findings of the reduced V_{oc} in P3HT-COOH-based devices compared to those using PTAA which, due to its deeper Fermi level, presents a larger electron extraction barrier and therefore reduces recombination losses.

4. Conclusions

Here, the PTAA, P3HT and P3HT-COOH compounds have been tested as passivation layers for the Cu:NiO_x material, which can play a role of the HTL in PSCs. The studies of a contact angle have shown that a sample with the perovskite precursor solvent (DMF:DMSO) dropped on the P3HT-COOH film has the lowest contact angle in a comparison to samples with other passivation materials. As a consequence, a smoother perovskite surface was obtained on the P3HT-COOH layer. The photoluminescence spectra measured for the HTL/perovskite structures prepared with different passivation materials indicate the best quenching efficiency for samples with P3HT-COOH, which is associated with a fast hole transfer from a perovskite to HTL. The solar cells with P3HT-COOH shows the lowest hysteresis index and the highest power conversion efficiency. Results obtained for PSCs with PTAA also look promising. However, a high cost of this passivation compound causes that P3HT-COOH seems to be a much more attractive material to construct efficient PSCs.

CRediT authorship contribution statement

Jędrzej Szmytkowski: Writing – original draft, Visualization, Validation, Formal analysis, Data curation. **Cheng-Gang Huang:** Writing – review & editing, Visualization, Validation, Resources, Investigation, Formal analysis. **Satish Bykkam:** Writing – review & editing, Formal analysis. **Damian Glowienka:** Writing – original draft, Visualization, Validation, Software, Resources, Investigation, Funding acquisition, Formal analysis. **Yulia Galagan:** Writing – review & editing, Supervision, Funding acquisition, Formal analysis, Conceptualization.

Declaration of competing interest

The authors declare that they have no known competing financial interests or personal relationships that could have appeared to influence the work reported in this paper.

Acknowledgments

This research was funded in part by National Science Centre, in cooperation with the M-ERA.NET 3 Call 2021 for the grant number 2021/03/Y/ST5/00233. This project has received funding from the European Unions Horizon 2020 research and innovation program under grant agreement No 958174. The authors wish to thank the Academic Computer Centre (CI TASK) in Gdańsk for providing the opportunity to carry out calculations.

Appendix A. Supplementary data

Supplementary material related to this article can be found online at https://doi.org/10.1016/j.solener.2025.113817.

Data availability

Data will be made available on request.

References

[1] J.J. Yoo, S.S. Shin, J. Seo, Toward efficient perovskite solar cells: Progress, strategies, and perspectives, ACS Energy Lett. 7 (2022) 2084–2091.
[2] D.I. Kim, J.W. Lee, R.H. Jeong, J.H. Boo, A high-efficiency and stable perovskite solar cell fabricated in ambient air using a polyaniline passivation layer, Sci. Rep. 12 (2022) 697.
[3] D. Glowienka, D. Zhang, F. Di Giacomo, M. Najafi, S. Veenstra, J. Szmytkowski, Y. Galagan, Role of surface recombination in perovskite solar cells at the interface of HTL/$CH_3NH_3PbI_3$, Nano Energy 67 (2020) 104186.
[4] Y. Wang, L. Duan, M. Zhang, Z. Hameiri, X. Liu, Y. Bai, X. Hao, PTAA as efficient hole transport materials in perovskite solar cells: A review, Sol. RRL 6 (2022) 2200234.
[5] R.H. Lohwasser, J. Bandara, M. Thelakkat, Tailor-made synthesis of poly(3-hexylthiophene) with carboxylic end groups and its application as a polymer sensitizer in solid-state dye-sensitized solar cells, J. Mater. Chem. 19 (2009) 4126–4130.
[6] J. Weickert, F. Auras, T. Bein, L. Schmidt-Mende, Characterization of interfacial modifiers for hybrid solar cells, J. Phys. Chem. C 115 (2011) 15081–15088.
[7] Q. Liao, Y. Wang, X. Yao, M. Su, B. Li, H. Sun, J. Huang, X. Guo, A dual-functional conjugated polymer as an efficient hole-transporting layer for high-performance inverted perovskite solar cells, ACS Appl. Mater. Interfaces 13 (2021) 16744–16753.

[8] L. Chu, L.M. Ding, Self-assembled monolayers in perovskite solar cells, J. Semicond. 42 (2021) 090202.
[9] W. Li, E. Martinez-Ferrero, E. Palomares, Self-assembled molecules as selective contacts for efficient and stable perovskite solar cells, Mater. Chem. Front. 8 (2024) 681–699.
[10] T.S. Balaban, Tailoring porphyrins and chlorins for self-assembly in biomimetic artificial antenna systems, Acc. Chem. Res. 38 (2005) 612.
[11] T. Miyatake, H.J. Tamiaki, Self-aggregates of bacteriochlorophylls c, d and e in a light-harvesting antenna system of green photosynthetic bacteria: Effect of stereochemistry at the chiral 3-(1-hydroxyethyl) group on the supramolecular arrangement of chlorophyllous pigments, Photochem. Photobiol. C 6 (2005) 89.
[12] A. Huijser, P.L. Marek, T.J. Savenije, L.D.A. Siebbeles, T. Scherer, R. Hauschild, J. Szmytkowski, H. Kalt, H. Hahn, T.S. Balaban, Photosensitization of TiO_2 and SnO_2 by artificial self-assembling mimics of the natural chlorosomal bacteriochlorophylls, J. Phys. Chem. C 111 (2007) 11726–11733.
[13] M.C. Balaban, A. Eichhofer, G. Buth, R. Hauschild, J. Szmytkowski, H. Kalt, T.S. Balaban, Programmed metalloporphyrins for self-assembly within light-harvesting stacks: (5, 15-dicyano-10, 20-bis(3, 5-di-tert-butylphenyl)porphyrinato)zinc(II) and its push-pull 15-N, N-dialkylamino-5-cyano congeners obtained by a facile direct amination, J. Phys. Chem. B 112 (2008) 5512–5521.
[14] T. Jochum, C.M. Reddy, A. Eichhofer, G. Buth, J. Szmytkowski, H. Kalt, D. Moss, T.S. Balaban, The supramolecular organization of self-assembling chlorosomal bacteriochlorophyll c, d, or e mimics, Proc. Natl. Acad. Sci. USA 105 (2008) 12736–12741.
[15] J. Szmytkowski, J. Conradt, H. Kuhn, C.M. Reddy, M.C. Balaban, T.S. Balaban, H. Kalt, Self-assemblies of novel magnesium porphyrins mimicking natural chlorosomal bacteriochlorophylls, J. Phys. Chem. C 115 (2011) 8832–8839.
[16] M. Koepf, J. Conradt, J. Szmytkowski, J.A. Wytko, L. Allouche, H. Kalt, T.S. Balaban, J. Weiss, Highly linear self-assembled porphyrin wires, Inorg. Chem. 50 (2011) 6073–6082.
[17] C.-Y. Chang, H.-H. Huang, H. Tsai, S.-L. Lin, P.-H. Liu, W. Chen, F.-C. Hsu, W. Nie, Y.-F. Chen, L. Wang, Facile fabrication of self-assembly functionalized polythiophene hole transporting layer for high performance perovskite solar cells, Adv. Sci. 8 (2021) 2002718.
[18] J.-Y. Lin, F.-C. Hsu, C.-Y. Chang, Y.-F. Chen, Self-assembled polar hole-transport monolayer for high-performance perovskite photodetectors, J. Mater. Chem. C 9 (2021) 5190.
[19] D. Glowienka, F. Di Giacomo, M. Najafi, I. Dogan, A. Mameli, F.J.M. Colberts, J. Szmytkowski, Y. Galagan, Effect of different bromine sources on the dual cation mixed halide perovskite solar cells, ACS Appl. Energy Mater. 3 (2020) 8285–8294.
[20] J. Szmytkowski, D. Glowienka, M. Verger, H. Gorter, I. Dogan, W. Verhees, M. Najafi, S. Veenstra, Y. Galagan, Additive effect of bromides and chlorides on the performance of perovskite solar cells fabricated via sequential deposition, J. Power Sources 513 (2021) 230528.
[21] J. Szmytkowski, Y. Galagan, D. Glowienka, Exploring the interfacial effects at the ETL/perovskite boundary in the semitransparent perovskite solar cells, Sol. Energy 266 (2023) 112176.
[22] D. Glowienka, J. Szmytkowski, Numerical modeling of exciton impact in two crystalographic phases of the organo-lead halide perovskite ($CH_3NH_3PbI_3$) solar cell, Semicond. Sci. Technol. 34 (2019) 035018.
[23] A. Castro-Carranza, J.C. Nolasco, M. Estrada, R. Gwoziecki, M. Benwadih, Y. Xu, A. Cerdeira, L.F. Marsal, G. Ghibaudo, B. Iniguez, J. Pallares, Effect of density of states on mobility in small-molecule n-type organic thin-film transistors based on a perylene diimide, IEEE Electron Device Lett. 33 (2012) 1201–1203.
[24] N. Tsutsumi, K. Kinashi, K. Masumura, K. Kono, Photorefractive performance of poly(triarylamine)-based polymer composites: An approach from the photoconductive properties, J. Polym. Sci. B 53 (2015) 502–508.
[25] G. Chen, F. Zhang, M. Liu, J. Song, J. Lian, P. Zeng, H.-L. Yip, W. Yang, B. Zhang, Y. Cao, Fabrication of high-performance and low-hysteresis lead halide perovskite solar cells by utilizing a versatile alcohol-soluble bispyridinium salt as an efficient cathode modifier, J. Mater. Chem. A 5 (2017) 17943–17953.
[26] T.S. Sherkar, C. Momblona, L. Gil-Escrig, H.J. Bolink, L.J.A. Koster, Improving perovskite solar cells: Insights from a validated device model, Adv. Energy Mater. 7 (2017) 1602432.
[27] G. Garcia-Belmonte, A. Munar, E.M. Barea, J. Bisquert, I. Ugarte, R. Pacios, Charge carrier mobility and lifetime of organic bulk heterojunctions analyzed by impedance spectroscopy, Org. Electron. 9 (2008) 847–851.
[28] R.C.I. MacKenzie, T. Kirchartz, G.F.A. Dibb, J. Nelson, Modeling nongeminate recombination in P3HT:PCBM solar cells, J. Phys. Chem. C 115 (2011) 9806–9813.
[29] D.B. Khadka, Y. Shirai, M. Yanagida, J.W. Ryan, K. Miyano, Exploring the effects of interfacial carrier transport layers on device performance and optoelectronic properties of planar perovskite solar cells, J. Mater. Chem. C 5 (2017) 8819–8827.
[30] G. Juska, K. Genevicius, N. Nekrasas, G. Sliauzys, G. Dennler, Trimolecular recombination in polythiophene: Fullerene bulk heterojunction solar cells, Appl. Phys. Lett. 93 (2008) 143303.
[31] F. Brivio, K.T. Butler, A. Walsh, M. van Schilfgaarde, Relativistic quasiparticle self-consistent electronic structure of hybrid halide perovskite photovoltaic absorbers, Phys. Rev. B 89 (2014) 155204.
[32] L.A.A. Pettersson, L.S. Roman, O. Inganäs, Modeling photocurrent action spectra of photovoltaic devices based on organic thin films, J. Appl. Phys. 86 (1999) 487–496.
[33] G.F. Burkhard, E.T. Hoke, M.D. McGehee, Accounting for interference, scattering, and electrode absorption to make accurate internal quantum efficiency measurements in organic and other thin solar cells, Adv. Mater. 22 (2010) 3293–3297.
[34] D. Glowienka, C.M. Tsai, A. Sbai, D. Luo, P.H. Lee, S.H. Huang, C.F. Li, H.W. Wang, G.S. Liou, J. Guthmuller, W.F. Su, Improving the efficiency of semitransparent perovskite solar cell using down-conversion coating, ACS Appl. Mater. Interfaces 16 (2024) 63528–63539.
[35] D. Glowienka, Y. Galagan, Light intensity analysis of photovoltaic parameters for perovskite solar cells, Adv. Mater. 34 (2022) 2105920.
[36] D. Madadi, I. Gharibshahian, A.A. Orouji, High performance a-$FAPbI_3$ perovskite solar cells with an optimized interface energy band alignment by a Zn(O, S) electron transport layer, J. Mater. Sci. Mater. Electron. 34 (2023) 51.